Diffuse emission of CO_2 and convective heat release at Nisyros caldera (Greece)

Giulio Bini[1], Giovanni Chiodini[2]*, Carlo Cardellini[3], Georges E. Vougioukalakis[4], Olivier Bachmann[1]

1- Institute of Geochemistry and Petrology, ETH Zürich, Clausiusstrasse 25, 8092 Zürich, Switzerland

2- Istituto Nazionale di Geofisica e Vulcanologia, sezione di Bologna, via D. Creti 12, 40128 Bologna, Italy

3 - Dipartimento di Fisica e Geologia, Università degli Studi di Perugia, via Pascoli snc, 06123, Perugia, Italy

4- Institute of Geology and Mineral Exploration, S. Lui 1, Olympic Village, Aharne, 13677 Athens, Greece

* Corresponding author: Giovanni Chiodini: giovanni.chiodini@ingv.it

Abstract

The diffuse emission of CO_2 from the south east sector of Nisyros caldera (Lakki plain) has been measured during a detailed survey (~ 1400 soil CO_2 flux measurements) performed in October 2018. The gas emissions are fed by hydrothermal sources and, in minor part, by the soil biogenic activity whose mean CO_2 flux (4 g m^{-2} d^{-1}) is here estimated for the first time. The total amount of hydrothermal CO_2 reaches 92 ± 8 t/d, a value that is slightly higher than that estimated with the same method between 1999 and 2001 (74 ± 7 t/d). The gas is emitted by different diffuse degassing structures (DDSs), including volcanic-hydrothermal structures (craters and domes) and NE-SW and NW-SE-trending tectonic lineaments.

Even if the total CO_2 emission is not particularly high at Nisyros (close to the median of CO_2 emissions measured in volcanoes worldwide), the process is very energetic. The thermal energy associated with the shallow condensation of the steam in the DDSs reaches ~ 60 MW, while we estimate at 134-270 MW the total amount of thermal energy involved in the convective rising of the deep geothermal liquids that transport the gas from the depth toward the surface. This large flux of energy could dramatically increase during future earthquakes by addition of heat and mass from a deep hydrothermal reservoir, potentially triggering hydrothermal explosions, as it happened several times in the past few centuries.

Keywords: Nisyros Caldera; CO_2 diffuse degassing; Thermal energy; Convective hydrothermal systems

1. Introduction

Carbon dioxide (CO_2) is one of the most abundant volatiles emitted from volcanic areas. Plumes, fumaroles, crater lakes and degassing grounds supply high amounts of deep-originated CO_2 (either magmatic or metamorphic) into the atmosphere (e.g., Perez et al., 2011; Burton et al.; 2013, Aiuppa et al., 2015; Cardellini et al., 2017). Volcanic CO_2 degassing is controlled by many factors, including the presence in the subsurface of magmatic or hydrothermal sources and factors affecting the permeability (such as the structural features and rock porosities, e.g., Chiodini et al., 2001; Caliro et al., 2005; Pérez et al., 2013; Viveiros et al., 2010). During volcanic crises, plumes and fumarolic vents release high amounts of volatiles, but even during periods of dormancy, volcanoes emit significant quantity of gases. In particular, CO_2 diffuse degassing from soil represents an important process to be considered during these dormant stages (Chiodini et al., 1998; Perez et al., 2013; Cardellini et al., 2017). Indeed, due to its relatively low solubility in silicate melt and its relatively non-reactive behaviour, CO_2 can be used to investigate the dynamics of deep degassing (e.g., Gerlach et al., 1997; Poland et al., 2012; Aiuppa et al., 2013). Measuring CO_2 from diffuse soil emanations can be particularly informative in volcanic edifices or calderas associated with large hydrothermal systems, where fluids are discharged from several locations, and where the acidic soluble gas species (e.g. SO_2, HCl, HF) are dissolved in the aquifer (Hernandez et al., 1998; Mori et al., 2001; Frondini et al., 2004; Bloomberg et al., 2014; Werner et al., 2014; Cardellini et al., 2017). In such scenarios, periodical measurements of ground CO_2 fluxes from large areas may be a key monitoring tool to follow the evolution of volcanic systems by tracking the variations of the total output and migration/changing of the main diffuse degassing structures (DDS) (e.g., Chiodini et al., 2010; Perez et. al., 2013; Cardellini et al., 2017). In addition, CO_2 flux anomalies allow to identify and map hidden tectonic and volcanic structures (e.g., faults, fractures and crater rims) when acting as preferential pathways for the ascent of magmatic/hydrothermal fluids (e.g. Barberi and Carapezza, 1994; Giammanco et al., 1998; Chiodini et al., 2001; Baubron et al., 2002; Aiuppa et al., 2004; Chiodini et al., 2004; Werner and Cardellini, 2006; Schütze et al., 2012).

At Nisyros Volcano, soil diffuse degassing of hydrothermal CO_2 affects a large part of the eastern sector of the caldera (Lakki plain, Fig.1b) that has been the location of historical hydrothermal eruptions. Previous detailed studies in the 1996-2001 period has provided a complex picture of CO_2 degassing, being emitted from hydrothermal craters, volcanic domes, faults and fractures (Brombach et al., 2001; Cardellini et al., 2003; Caliro et al., 2005). Here we present the result of a new detailed soil CO_2 flux campaign, performed in October 2018 (~ 1400 measurements over an area of 2.2 km^2). A main aim is to check for eventual variations in the amount of emitted CO_2 and in the geometry of the diffuse degassing structures (DDS) with respect to the results of several campaigns performed in the 1999-2001 period in the frame of GEOWARN project (GEOWARN, 2003; Cardellini et al., 2003; Caliro et al., 2005).

Recently, soil CO_2 flux measurements have found useful applications in geothermal studies for geothermometric purposes (Harvey et al., 2017), for environmental monitoring and health risk assessment (Viveiros et al., 2010; Bergfeld et al., 2015), and to evaluate the thermal energy emitted by hydrothermal systems (Fridrikson et al., 2006; Chiodini et al., 2007; Bloomberg et al., 2014; Harvey et al., 2015). In this frame, a second objective of the work is to compute, for the first time, the H_2O mass and thermal budgets of the entire process (from depth to the surface) using the measured CO_2 emission as a tracer of the original liquids convectively rising at Lakki plain.

1.1 Volcanic-hydrothermal setting and recent activity of the volcano

Nisyros volcano belongs to a group of volcanic islands (including Kos, Yali, and other minor islands; Di Paola, 1974; Francalanci et al., 1995; Vougioukalakis, 1998), in the easternmost edge of the active Aegean arc (Fig. 1a). Volcanism in the Kos-Nisyros-Yali volcanic complex started at least 3 Ma ago (Matsuda et al., 1999; Bachmann et al., 2010), and erupted a number of units (both explosive and effusive) until recent times (e.g., see summary in Pe-Piper & Piper, 2002); the youngest eruptions were probably located on Yali and Nisyros, with pumice fall and lava domes/flows dating back to < 30-25 kyr (Wagner et al., 1976; Federman and Carey, 1980). The Kos-Nisyros-Yali volcanic field is characterized by a large caldera-forming eruption at ~160-165 Kyr (Smith et al., 1996; Bachmann et al., 2010), which formed the (> 60 km^3 D.R.E) Kos Plateau Tuff (KPT).

Nisyros volcano sits on the southern edge of the 5-10 km wide caldera that collapsed during the KPT, and all its subaerial units appear younger than the KPT (see summary in Bachmann et al., 2010). The activity of the volcano is dominated by 2 large explosive eruptions, the Lower and Upper Pumice (Fig. 1b), likely a few km^3 Dense Rock Equivalent (DRE) each (e.g., Longchamp et al., 2011). These eruptions built a ~4 km-diameter collapse structure in the center of the island that was partly flanked and subsequently filled by large lava flows of dacite to rhyodacitic composition. The most recent activity of the volcano is characterized by historical hydrothermal eruptions that occurred in the southern half of the Lakki plain (Fig. 1b), the last of which led to the formation of Polybote Micros crater in 1887 (Marini et al., 1993).

At Lakki plain, hot altered grounds, bubbling/mud pools and fumaroles represent the surface manifestations of a still active hydrothermal circulation. The data of the two deep wells Nis-1 and Nis- 2 (Fig. 1b), together with the geochemical interpretation of the fumarolic fluids and thermal springs, indicate the presence of a shallow (at depths of 250-700 m, T < 250°C) and a deep (at depth >1000-1500 m, T > 290°C) aquifer beneath the Lakki plain (Chiodini et al., 1993; Brombach et al., 2003). According to Marini et al. (1993), the sudden injection of the deeper hotter fluids into the shallower aquifer, caused by local volcano-tectonic earthquakes, could be the trigger of the hydrothermal explosions that occurred in the area. Following this model, it is likely that the seismic crisis occurred in 1996-1997 (Papadopoulos et al., 1998; Sachpazi et al., 2002) led to variations in the chemical composition of the fumaroles, as a consequence of the input of hot, sulphur-rich deep fluids into the shallower part of the hydrothermal system (Chiodini et al., 2002).

Between 2001 and 2002, two collapse events occurred in the northern part of the Lakki plain, leading to the formation of a 600 m long fissure. Based on the chemical (e.g. H_2S, CH_4, H_2) and isotopic ($\delta^{13}C$-CO_2) composition of the interstitial gases collected at 40 cm depth from the bottom of the fracture, as well as the chemical and mineralogical features of the fissure wall deposits, Venturi et al. (2018) suggest that the circulation of acidic fluids (CO_2- and H_2S-rich) may have weakened the terrain, triggering such collapses. In this frame, we carried out detailed CO_2 flux measurements along the bottom of this fracture to highlight the eventual occurrence of anomalous degassing.

2. Materials and methods

2.1 Soil CO_2 flux

Soil CO_2 fluxes were measured over an area of 2.2 km^2, roughly corresponding to the central and southern parts of the Lakki plain (Fig. 1b), during a survey carried out from 1 to 14 October 2018. In order to obtain a high resolution of the main structures, we adopted a measurement density of about 1 every 1700 m^2. The entire data set consists of 1437 points (Fig. 3), which includes also data form detailed surveying of Stefanos crater (80 points), of the fracture opened in 2001-2002 (30 points), and of a NW-SE lineament (89 points) located in the northern part of the studied area (Appendix a).

The measurements were performed using the accumulation chamber method (AC; Chiodini et al., 1998). The instrument we used was developed at Perugia University (Italy) and it is composed of (i) a metal cylindrical chamber (volume-chamber of 2.8 L), (ii) an infrared sensor (LICOR Li-820, working in the range 0-20,000 ppm of CO_2), (iii) an analog-digital converter and a (iv) smartphone (see Fig. S4 Cardellini et al., 2017). The chamber is placed on the ground and the gas is pumped from the chamber, at a rate of ~0.0167 L s^{-1}, into the sensor. After passing through the infrared spectrophotometer, the gas is reinjected into the chamber through a perforated manifold in order to avoid depressurization and to homogenize the gas inside the chamber (Cardellini et al., 2017). The analogic signal from the infrared sensor is then digitally converted and saved on a smartphone through Bluetooth connection. Using the Gasdroide app (Cardellini et al., 2017), the device plots the CO_2 concentration (C_{CO2}) over time and allows to compute in real time the rate of increase of CO_2 in the chamber ($\alpha = dC_{CO2}/dt$), i.e. the initial slope of the C_{CO2}-t curve. The flux of CO_2 from soil is proportional to α and a geometric factor, c*f*, theoretically the height of the chamber (see Chiodini et al., 1998 for further details), according to the relation $\varphi_{soil\ CO2} = cf \times \alpha$. The c*f* of the used apparatus was determined by an instrumental calibration test carried out in laboratory at Perugia University before the survey (see Chiodini et al., 1998; Cardellini et al., 2017 for further details on calibration procedure).

The measured CO_2 fluxes were elaborated by statistical and geostatistical tools (i.e. GSA method and sequential Gaussian simulations). The GSA method (Graphical Statistical Approach, Chiodini et al., 1998) was used in order to distinguish the main sources of the soil CO_2 flux (i.e. biological vs. volcanic). In fact, the multiple origin of the CO_2 can result in a polymodal statistical distribution of CO_2 flux values, which plots as a curve with $n-1$ inflection points on a logarithmic probability plot when n log-normal distributed populations overlap (Sinclair, 1974; Chiodini et al., 1998; Cardellini et al., 2003). According to Sinclair (1974), a graphical method can be used for the partition of such complex statistical distributions into individual log-normal populations and compute the fraction (f_i), the mean (M_i) and the standard deviation of each of them. The same approach was used to elaborate the data of isotopic composition of the soil CO_2 provided by Venturi et al. (2018). Since the computed M_i value for the CO_2 flux refers to the logarithm of the CO_2 flux values, the mean value of CO_2 flux was then estimated using a Montecarlo simulation procedure. The results of the Montecarlo simulation procedure were also used to define the uncertainty of the estimated mean CO_2 flux values as the standard deviation of n simulated values.

In order to (1) characterize the spatial distribution CO_2 fluxes, (2) map the soil CO_2 degassing and (3) estimate the total CO_2 output, a geostatistical approach based on sequential Gaussian simulations (sGs method) was used. The sGs method is based on the *sgsim* algorithm of the GSLIB software library (Deutsch and Journel, 1998) and was first proposed for the study of soil CO_2 diffuse degassing by Cardellini et al. (2003). It consists of the production of numerous equiprobable realizations of the spatial distribution of CO_2 flux (i.e. CO_2 flux maps). The CO_2 flux values were simulated at locations defined by a regular grid in order to reproduce the CO_2 flux statistical distribution and the CO_2 flux spatial structure (i.e., the variogram of the CO_2 flux; Appendix b). The simulations were run in order to produce 200 realizations for each dataset. The produced realizations were post-processed to realize maps of the CO_2 flux and probability maps. The map of CO_2 flux was obtained through a pointwise linear average of all the realizations. The probability map consists in a map of the probability that, among all the realizations, the simulated CO_2 flux at any location (i.e. at grid nodes) is above a cut-off value.

We applied the same elaborations also to the data of five surveys performed in September 1999, May 2000, September 2000, June 2001 and September 2001 (1999-2001 survey in the following, Caliro et al., 2005). The 2018 campaign and the 1999-2001 survey were carried out during dry periods when the soil water content, the main parameter which could affect the diffusion of gases (e.g. Viveiros et al., 2008), is not altered by the rain.

2.2 From CO_2 flux to H_2O mass and energy budgets

Kerrick et al. (1995) considered a convective model for the transfer of heat and CO_2 in the Taupo geothermal area to compute the CO_2 flux starting from heat flux, temperature and CO_2 content of the deep geothermal liquids. Later, the same conceptual model of the convective ascent of deep fluids transporting heat and CO_2 was used to estimate the thermal energy involved in the CO_2 degassing process at Reykjanes geothermal area (Island, Fridrikson et al., 2006) and at Latera caldera (Italy, Chiodini et al., 2007). According to this convective model, we can assume that the hydrothermal CO_2 currently emitted at Lakki plain is originally dissolved in deep geothermal liquids and released during their ascent, depressurization and boiling. Based on this conceptual model (Fig. 2), on the measured CO_2 fluxes, and on assumptions suitable for the Nisyros case (see the results section), we estimated the mass flux (Q_i) and the associated thermal energies (QH_i) of the deep hydrothermal liquid (Q_{L0}, QH_{L0}), and of the steam that separates with the CO_2 during the boiling process and condenses approaching the surface (Q_{cond}, QH_{cond}).

The mass flux of the condensates, i.e. Q_{cond} (in kg/s), and the associated thermal energy, i.e. QH_{cond} (latent heat of condensation plus cooling of the condensates at ambient temperature, in MW), are given by:

$$Q_{cond} = Q_{CO2} \times R_{H2O/CO2} \qquad (1)$$

$$QH_{cond} = Q_{cond} \times (H_{V,\,100°C} - H_{L,\,20°C}) \times 0.001 \qquad (2)$$

where Q_{CO2} is the CO_2 output (in kg/s), $R_{H2O/CO2}$ is the H_2O/CO_2 weight ratio of the fumaroles located in the degassing CO_2 areas (Chiodini et al., 2005), $HV_{,\,100°C}$ and $H_{L,\,20°C}$ are the enthalpies of the steam at 100 °C and of the liquid at ambient temperature (2676 kJ/kg and 83.9 kJ/kg, respectively; Keenan et al., 1969), and 0.001 is the factor to convert kW in MW. Note that the assumption of a condensation at 100° C is supported by the observation that the temperature of the hot soils degassing CO_2 increases with depth up to reach the boiling temperature of the water (~ 100°C) while, at higher depths, it remains constant (see Chiodini et al., 2005 and references therein).

The mass flux of the geothermal liquid Q_{L0} (kg/s) and the associated thermal energy QH_{L0} (MW) are computed, as follows:

$$Q_{L0}= Q_{CO2}/m_{CO2,d} \qquad (3)$$

$$QH_{L0} = Q_{L0} \times H_{L,T0} \times 0.001 \qquad (4)$$

where Q_{CO2} (in mol/s) is the CO_2 output, $m_{CO2,d}$ (mol/kg) is the concentration of the degassed CO_2 originally dissolved in the liquid (Chiodini et al., 2007), $H_{L,T0}$ (kJ/kg) is the enthalpy of the liquid at the original temperature T_0, and 0.001 is the factor to convert kW in MW.

The difference $Q_{res} = Q_{L0}-Q_{cond}$ includes the mass of the residual liquid remaining after boiling and of the steam that condense in the subsurface (lateral outflow or descending column of the convective cells) while the difference $QH_{res} = QH_{L0}-QH_{cond}$ is the sum of the others terms of the energy balance (e.g., the thermal energy transported by the lateral outflow, the energy transmitted to the media to maintain hot the system, etc.)

In the case of Nisyros, the variables of the equations 1 to 4 were estimated, as follow:

Q_{CO2}: computed from soil CO_2 flux measurements;

$R_{H2O/CO2}$: was set as the H_2O/CO_2 mean weight ratio of the fumaroles located within the zones degassing CO_2, the compositions of which are available in the literature (Chiodini et al., 1993; Brombach et al., 2003; Caliro et al., 2005; Appendix c);

T_0: the temperature of the original geothermal liquids was assumed as that estimated for the deep reservoirs reached by the geothermal wells Nis-1 and Nis-2 (340°C and 290°C, respectively; Marini and Fiebig, 2005);

$m_{CO2,d}$: the CO_2 molalities estimated from preliminary tests of the wells Nis-1 (m_{CO2} = 0.29 mol/kg at 340°C) and Nis-2 (m_{CO2} = 0.12 mol/kg at 290°C, see Table 9.2 in Marini and Fiebig, 2005) were selected as the most suitable proxy for the CO_2 concentration in the original deep liquids ($m_{CO2,L0}$). We also assumed that the CO_2 is completely degassed during the ascent and the depressurization of the deep fluids (i.e. $m_{CO2,d}$.= $m_{CO2,L0}$).

3. Results

3.1 Hydrothermal CO_2 output at Lakki plain

3.1.1 Background estimation and total output of hydrothermal CO_2

The measured soil CO_2 flux varies from 0.07 g m^{-2} d^{-1} to 3725 g m^{-2} d^{-1} with a mean value of 55 g m^{-2} d^{-1}. The data were used to map the soil CO_2 flux (Fig. 3) and to estimate the total CO_2 output and its uncertainty applying the sGs method (see section 2.1). The obtained total CO_2 output of 100.6 ± 7.9 t/d (Table 1) includes both the gas produced by the biological activity in the soil (background flux) and the gas supplied by the hydrothermal source. The background flux was estimated by two approaches based on independent data sets:

1. The first approach is based on the selection of measurements from the northern part of the investigated area (288 measurements, see rectangular area in Fig. 3) where low fluxes (blue colour) dominate. In the log-probability plot of Fig. 4a, these data describe a curve with 2 inflation points indicating the overlapping of 3 populations. The lowest flux Population A (f_A = 0.07, mean = 0.59 ± 0.08 g m^{-2} d^{-1}) is representative of the degassing of soils with scarce or null vegetation, a consideration that is supported by both the very low fluxes and field observations. The highest flux Population C (f_C = 0.35, mean = 32.7 ± 3.9 g m^{-2} d^{-1}) represents outlets the hydrothermal source (see next sections), whereas the Population B (f_B = 0.58, mean = 3.96 ± 0.20 g m^{-2} d^{-1}) reflects the background fluxes fed by soil biogenic activity.
2. The second approach is based on the results of a soil CO_2 prospecting available in the literature (Venturi et al., 2018). The work, among other parameters, reports 50 carbon isotopic compositions of soil CO_2 at a depth of 40 cm and as many measurements of soil CO_2 fluxes performed in the same sites. In the probability plot of Fig. 4b, the $\delta^{13}C$ values are again interpretable with the overlapping of 3 populations. The population with the highest values ($\delta^{13}C$ = -1.6‰ ± 0.8‰) is easily identified as the hydrothermal CO_2 as it is characterised by an isotopic signature close to the that of the fumarolic CO_2 ($\delta^{13}C$ from -1‰ to -1.4‰, Venturi et al., 2018; $\delta^{13}C$ from -0.4‰ to -4‰, Brombach et al., 2003). The population with the lowest values ($\delta^{13}C$ = -22.3‰ ± 1.5‰) is produced by the soil biogenic CO_2 as clearly indicated by the negative values that are close to the biologically derived carbon (see Chiodini et al. 2008 and references therein). Both the hydrothermal and soil biogenic populations are characterised by a low variance suggesting that the values that are intermediate between them cannot be ascribed to the overlapping of the two populations but rather to the occurrence of the physical mixing between the two sources (the third population, mixing of the two sources in Fig. 3b, $\delta^{13}C$ = -12.6‰ ± 5‰). The CO_2 fluxes associated with the soil biogenic CO_2 population 3 vary from 0.03 $gm^{-2}d^{-1}$ to 14.9 $gm^{-2}d^{-1}$ with a mean value of 4 $gm^{-2}d^{-1}$.

The two independent methods give comparable results, indicating a mean CO_2 production from soil biogenic activity of ~ 4 g m^{-2} d^{-1}. This value is relatively low in comparison with measurements in other hydrothermal areas of the world (e.g. Table 3 in Harvey et al., 2015; Viveiros et al., 2010), but expected considering the scarce vegetation and/or the presence of bare soils. This biogenic-background value allowed us to estimate an output of ~8 t/d of biogenic CO_2 for the entire surveyed area and to obtain a value of ~92 t/d for the total CO_2 output from the hydrothermal source. This estimate of the flux produced by the hydrothermal source has to be considered a minimum value, since the biogenic CO_2 flux of 4 g m^{-2} d^{-1} has been estimated in the northern zone, which is the most vegetated area. The total hydrothermal CO_2 output obtained for the 2018 survey is ~24% higher than that obtained, adopting the same approach, for the 1999-2001 survey (Table 1; Caliro et al., 2005)

3.1.2 Probability maps and definition of the DDSs

In order to define the locations where the hydrothermal source fed the soil CO_2 flux (i.e. the DDSs), we first defined a maximum threshold for the CO_2 flux generated by the soil biogenic source alone. We selected a precautionary threshold of 15 g d^{-1} m^{-2} above which < 1% of the background flux population B belongs (Fig. 4a). The DDSs were defined as those areas where the probability, among all the performed realizations, that the simulated CO_2 flux is higher than the biogenic CO_2 flux threshold is over 50% (Cardellini et al., 2003), i.e. the CO_2 flux is reasonably fed by the hydrothermal source. The probability maps for the 2018 and 1999-2001 surveys are shown in Fig. 5a and 5b respectively, and the computed extent of the DDSs is reported in Table1. The DDSs correspond to hydrothermal-volcanic structures (hydrothermal craters and domes) that are located along the fault bordering to the east and to the west the Lakki plain (Fig. 5) and, in the northern sector, to obvious NE-SW and NW-SE-trending lineaments likely of tectonic origin (Fig. 5).

In order to better define and understand such complex pattern of degassing structures, either linked to evident hydrothermal activity, or controlled by tectonics structures where no obvious thermal manifestations occur, we separately considered the following nine DDSs (Fig. 5): 1) the hydrothermal crater of Stefanos; 2) the hydrothermal craters of Kaminakia; 3) the hydrothermal craters of Polybote; 4) the hydrothermal crater of Phlegeton; 5) the Lofos dome; 6) the hydrothermal site of Ramos; 7) the NE fault bordering to the east the caldera floor; 8) and 9) the hundreds meters long lineaments of relatively high CO_2 flux located in the northern part of the studied area (NE-SW and NW-SE). For each of them, specific computations were carried out applying the same method used for the entire area, i.e. based on CO_2 flux maps for the estimation of the total output and on probability maps for the computation of the singular DDS extent (Appendix d) . The results are summarized in Table 2 and in Fig. 6 for both the 2018 and 1999-2001 datasets.

The nine DDSs differed in shape and magnitude of degassing. The Stefanos, Kaminakia and Lofos DDSs had the highest CO_2 outputs (10-20 t/d) whereas the lowest emissions were computed from the linear DDSs in the northern sector (8-NESW line and 9-NWSE line, 1-4 t/d, see Table 2 and Fig. 6). The hydrothermal CO_2 output was assumed equal to the total CO_2 output for the DDSs where no relevant vegetated soil is present (1-Stefanos, 2-Kaminakia, 3-Polybote, 4-Phlegeton, 5-Lofos dome, 6 Ramos), whereas the biogenic background correction was applied to the other zones (Table 2).

Particular attention was paid to the fracture area opened in 2001-2002, which is located in DDS no.8 (Fig. 5). Preliminary data processing, performed during the field work, showed that the measurement grid adopted did not allow us to highlight any CO_2 flux anomaly linked to the fracture. This consideration, supported by the final elaboration of the soil CO_2 flux data (Fig. 3 and Fig. 7a), suggested us to adopt a more detailed sampling along the entire 600 m long fracture (30 measurements in the bottom of the fracture, red points in Fig. 7b, c). The data set, integrated with these specific measurements, allowed us to highlight a weak CO_2 flux anomaly along the entire 600 m long fracture (Fig. 7b). All the measurements performed inside the fracture, even if not high in absolute, were indeed systematically higher than those performed outside the fracture (see transects *c1* to *c10* in Fig. 7c).

3.2 H_2O mass and energy budget of the convective hydrothermal system feeding the CO_2 emission

The total flux of condensed steam (Q_{cond}) and the associated thermal energy released through condensation and cooling (QH_{cond}), computed by summing the contribution of each DDS and scaling the results over the entire surveyed area (Table 3), are 23.4 kg/s and 60.7 MW, respectively. This latter value is higher than previous estimations (42.5 MW, Caliro et al., 2005), according to the increased emission of the deeply derived CO_2.

The computed amount of hot liquids (Q_{L0}) transporting from depth the CO_2 varies from 83.9 kg/s (Nis-1 case) to 209 kg/s (Nis-2 case) with associated thermal energies (QH_{L0}) from 134 MW to 270 MW. Most of this energy would be transported by the residual liquids that escape the system through a lateral outflow (and/or are possibly involved in the descending columns of the convective cells) and/or to heat the rocks of the system (QH_{res} from 74 to 211 MW). Numerous thermal springs located close to the coast (at sea level, Fig. 1b), discharge mixtures of a thermal component with sea water and groundwaters confirming the existence of a significant lateral outflow of geothermal liquids.

Discussion and Conclusions

One of the aims of our study was to check the eventual variations in the diffuse degassing process affecting the area over decadal timescales. In October 2018, the hydrothermal CO_2 emission at Lakki plain was of 91.6 t/d, close to the median diffuse emission of deep CO_2 from 73 worldwide volcanoes (112 t/d) that were measured and published in the last years and recently compiled in an open access database (Cardellini et al., 2013; www.magadb.net) and used for a review of volcanic CO_2 emissions (Werner et al., 2019). This CO_2 output for Nisyros is higher than a previous estimate (68 t/d Caliro et al., 2005). This increase is partially due to the different evaluation of the background contribution from the soil biogenic source that was assumed to be of 8 $gm^{-2}d^{-1}$ in Caliro et al. (2005). However, a new treatment of the soil flux data together with the elaboration of the carbon isotopic compositions of soil gases (data only recently available in the literature) indicated a value of 4 $gm^{-2}d^{-1}$ is more appropriate. Hence, the total 1999-2001 hydrothermal CO_2 output should be ~ 74 t/d after processing the data with the same methods applied to the 2018 datasets. This still leads to an imbalance of ~ 20 t/d between 1999-2001 and 2018 (from 74 to 92 t/d); the increase of the CO_2 emission in the 20 years is accompanied by the enlargement of the area degassing hydrothermal fluids (from 0.77 km^2 in 1999-2001 to 0.92 km^2 in 2018; Table 1). Although the 1999-2001 surveys were carried out with significantly higher number of measured points comparing to the 2018 campaign, the observed increase of ~ 24% can not be attributed to the different number of measurements. Indeed, the measurements number of both the surveys are sufficiently high to provide an estimation of the total CO_2 output with errors lower than 5% as predicted by applying the relation between the estimate uncertainty and the number of measurements within the DDS (see section 3.2.3 in Cardellini et al., 2003).

The changes in the diffuse emission of CO_2 were further investigated by dividing the area in nine DDSs (Fig. 6; Table 2). This detailed new treatment of the data shows that the enlargement of the areas degassing hydrothermal CO_2 affected almost all the DDSs (Fig. 6a), while the increase in the total emission results are less homogeneous (Fig. 6b). The strongest increases involve the Lofos dome (12.6 t/d in 1999-2001, 20 t/d in 2018; Table 2) and the hydrothermal site of Ramos (4.83 t/d in 1999-2001, 10.5 t/d in 2018; Table 2), whereas a significant decrease in the CO_2 output was observed at Kaminakia craters (20.8 t/d in 1999-2001, 12.8 t/d in 2018; Table 2). In other zones, the degassing process remained nearly constant (e.g., Stefanos crater with output of 14.7 t/d in 1999-2001 and 16.8 t/d in 2018; Table 2).

In general, the DDSs points to a strong structural control; they are located along the NE-SW faults that border to the east and to the west the Lakki plain or along NE-SW and NW-SE lineaments in the plain (Fig. 5), the latter corresponding to the two main directions of regional tectonics at Nisyros (Vougioukalakis, 1993). The role played by the local faults is particularly evident at

1. Lofos dome, where the degassing zone is limited by NE-SW and NW-SE rectilinear borders (Fig. 5), and
2. in the northern sector of the surveyed area, where CO_2 anomalies correspond to evident NE-SW and NW-SE lineaments likely of tectonic origin (Fig. 5).

Significant efforts were devoted to measure the CO_2 flux from the fracture that opened in 2001-2002 following the NE-SW and the NW-SE directions (Figs. 7). Previous investigations discovered hydrothermal gases (CO_2 and H_2S) in the soil of the fracture but did not highlight anomalies in the CO_2 emission (Venturi et. al, 2018). Here, after adopting a suitable measurement strategy, we show clear evidence of the anomalous CO_2 ascent from the entire 600 m long fracture (Fig. 7b). This new result agrees well with the presence at shallow depth of CO_2- and H_2S-rich fluids that alter the minerals of the rocks, cause self-sealing and permeability decrease (Venturi et al., 2018), hence preventing high gas fluxes. Such permeability reduction, possibly occurring within any fracture in the volcanic edifice of Nisyros, can be reversed by seismic activity. This process of reducing-increasing permeability could explain the gas flux fluctuations between 1999-2001 and 2018. Indeed, Nisyros is located in a seismically active area where, during this century, an average of 2.7 events per month with $M > 2.8$ was observed (Papadimitriu et al., 2017). In addition periods of enhanced seismicity occurred in 2011, 2014 (Papadimitriu et al. 2017) and 2017 (Kos earthquake M 6.6, Heidarzadehet al., 2017).

Assuming a convective model for the heat and the gas transfer, we computed the mass and heat fluxes of the ascending deep liquids (Q_{L0} = 84-209 kg/s; QH_{L0}= 134-270 MW) and the mass and thermal energy of the steam condensing at the surface (Q_{cond} = 23 kg/s; QH_{cond} = 61 MW). We stress that the Q_{L0} and QH_{Lo} estimations can be affected by uncertainties larger than those of Q_{cond} and QH_{cond}. The latter are in fact computed based only on measurements and on the observation of the presence of hot soils in the main degassing areas while the estimations of Q_{L0} and QH_{Lo} are dependent also on the original temperature and CO_2 concentration in the deep geothermal liquids. This information is not available in many hydrothermal degassing sites of the world or can only roughly be estimated. At Nisyros, we use temperatures and CO_2 concentrations estimated from preliminary tests of two wells (Nis-1 and Nis-2) that were never in production. We are confident, however, of the reliability of the data because they are close to those expected for typical geothermal systems as described by the empirical T- m_{CO2} relation of Arnorsson and Gunnlaugsson

(1985) (Fig. 8). Unfortunately, the flow rate of the undiluted thermal component transported by the springs, that could be used for independent estimations of mass and energy budget, is unknown. In spite of these uncertainties, the high Q_{L0} and QH_{Lo} estimates (84-209 kg/s; 134-270 MW) and the high values of the mass and heat of the shallow steam condensation (Q_{cond} = 23.4 kg/s; QH_{cond} = 60.7 MW) point to a very large amount of energy involved in the process that fed the CO_2 degassing. For example, the convective heat flux, computed by dividing only the measured Q_{cond} by the Nisyros island area (41 km^2), results at 1.6 W m^{-2} a value that is comparable to the convective heat flux at Yellowstone and higher than that estimated at Long Valley caldera (~ 2 W m^{-2} and ~ 0.6 W m^{-2}, respectively; Sorey, 1985)

The flux of deep liquids involved in the convection, currently estimated in hundreds of kg/s, could rise dramatically during the occurrence of earthquakes, as permeability increases. It was suggested that earthquake-related increase of the deep and hot fluid fluxes into the shallow aquifer could have caused hydrothermal explosions and the debris flows that originated the several craters of Lakki plain (Marini et al., 1993). This fault/earthquake-controlled mechanism for the genesis of the hydrothermal craters is in agreement with both the previous interpretation of the Nisyros hydrothermal craters and the historical chronicles of the most recent hydrothermal eruptions that occurred concurrently with strong earthquakes (Marini et al. 1993 and references therein). In this frame, of particular relevance is the NE-SW CO_2 anomaly (DDS 8 evident in both the 1999-2001 and 2018 data; Fig. 5) that does not correspond to any geological superficial feature, but is likely linked to a fault covered by the recent intra-caldera deposits of Lakki plain. The extension towards SW of this 800 m long lineament connects the northern part of Lakki plain to the hydrothermal crater of Stefanos, possibly highlighting a fault that in the past allowed the hot fluids of the deeper aquifer to transfer rapidly into the shallower levels, triggering the hydrothermal explosion that generated the crater.

In conclusion, the new maps and estimations of the CO_2 emission, the DDS by DDS treatment of the data, and the estimation of the H_2O mass balance and of the energy balance provide a detailed and comprehensive picture of the CO_2 degassing process currently affecting the Nisyros caldera.

The results obtained and the methods used can be useful to plan a future detailed monitoring system of the volcano, particularly in time of crisis. It can also find valuable applications in geothermal prospecting of convective hydrothermal systems and monitoring activity in other volcanic areas around the world.

Acknowledgments

We thank the editor, M. F. Viveiros and an anonimous reviewer for their insightful comments. This research was financed by the Swiss National Foundation grant 200021_178928.

References

Aiuppa, A., Fiorani, L., Santoro, S., Parracino, S., Nuvoli, M., Chiodini, G., Minopoli, C., Tamburello, G., 2015. New ground – based lidar enables volcanic CO_2 flux measurements. Sci. Rep. 5, 13614. doi:10.1038/srep13614.

Aiuppa, A., Caleca, A., Federico, C., Gurrieri, S., Valenza, M., 2004. Diffuse degassing of carbon dioxide at Somma-Vesuvius volcanic complex (Southern Italy) and its relation with regional tectonics. J. Volcanol. Geotherm. Res. 133, 55–79.

Aiuppa, A., Tamburello, G., Di Napoli, R., Cardellini, C., Chiodini, G., Giudice, G., Grassa, F., Pedone, M., 2013. First observations of the fumarolic gas output from a restless caldera: Implications for the current period of unrest (2005–2013) at Campi Flegrei, Geochem. Geophys. Geosyst. 14, 4153–4169. doi:10.1002/ggge.20261.

Arnorsson, S., Gunnlaugsson, E., 1985. New gas geothermometers for geothermal exploration-Calibration and application. Geochim. Cosmochim. Acta 49, 1307–1325.

Bachmann, O., Schoene, B., Schnyder, C., Spikings, R., 2010. $^{40}Ar/^{39}Ar$ and U/Pb dating of young rhyolites in the Kos-Nisyros volcanic complex, Eastern Aegean Arc (Greece): age discordance due to excess ^{40}Ar in biotite. Geochem. Geophys. Geosyst. 11, Q0AA08.

Barberi, F., Carapezza, M.L., 1994. Helium and CO_2 soil gas emission from Santorini (Greece). Bull. Volcanol. 56, 335-342.

Baubron, J. C., Rigo, A., Toutain, J. P., 2002. Soil gas profiles as a tool to characterise active tectonics areas: The Jaut Pass example (Pyrenees, France). Earth Planet. Sci. Lett. 196, 69–81.

Bergfeld, D., Vaughan, R.G., Evans, W. C., Olsen, E., 2015. Monitoring ground-surface heating during expansion of the Casa Diablo production well field at Mammoth Lakes, California. GRC Transactions 39, 1007-1013.

Bloomberg, S., Werner, C., Rissmann, C., Mazot, A., Horton, T., Gravley, D., Kennedy, B., Oze, C., 2014. Soil CO_2 emissions as a proxy for heat and mass flow assessment, Taupo Volcanic Zone, New Zealand. Geochem. Geophys. Geosyst. 15, 4885–4904. doi:10.1002/2014GC005327.

Brombach, T., Hunziker, J. C., Chiodini, G., Cardellini, C., Marini, L., 2001. Soil diffuse degassing and thermal energy fluxes from the southern Lakki plain, Nisyros (Greece). Geophys. Res. Lett. 28(1), 69–72.

Brombach, T., Caliro, S., Chiodini, G., Fiebig, J., Hunziker, J. C., Raco, B., 2003. Geochemical evidence for mixing of magmatic fluids with seawater, Nisyros hydrothermal system, Greece. Bull. Volcanol. 65, 505–516. doi: 10.1007/s00445-003-0278-x.

Burton, M. R., Sawyer, G. M., Granieri, D., 2013. Deep carbon emissions from volcanoes. Rev. Mineral. Geochem. 75, 323-354.

Cardellini, C., Chiodini, G., Frondini, F., 2003. Application of stochastic simulation to CO_2 flux from soil: Mapping and quantification of gas release. J. Geophys. Res. 108, 2425. doi: 10.1029/2002JB002165.

Cardellini, C., Chiodini, G., Frigeri, A., Bagnato, E., Aiuppa, A., Mc Cormick, B. T., 2013. The development of a new database of gas emissions: MAGA, a collaborative web environment for collecting data. American Geophysical Union, Fall Meeting 2013, San Francisco, USA, abstract id. V31B-2708 (2013).

Cardellini, C., Chiodini, G., Frondini, F., Avino, R., Bagnato, E., Caliro, S., Lelli, M., Rosiello, A., 2017. Monitoring diffuse volcanic degassing during volcanic unrests: The case of Campi Flegrei (Italy). Sci. Rep. 7, 6757. doi: 10.1038/s41598-017-06941-2.

Caliro, S., Chiodini, G., Galluzzo, D., Granieri, D., La Rocca, M., Ventura, G., 2005. Recent activity of Nisyros volcano (Greece) inferred from structural, geochemical and seismological data. Bull. Volcanol., 67, 358–369. doi:10.1007/s00445-004-0381-7.

Chiodini, G., Cioni, R., Leonis, C., Marini, L., Raco, B., 1993. Fluid geochemistry of Nisyros island, Dodecanese, Greece. J. Volcanol. Geotherm. Res. 56, 95–112.

Chiodini, G., Cioni, R., Guidi, M., Raco, B., Marini, L., 1998. Soil CO_2 flux measurements in volcanic and geothermal areas. Appl. Geochem. 13, 543–552.

Chiodini, G., Frondini, F., Cardellini, C., Granieri, D., Marini, L., Ventura, G., 2001. CO_2 degassing and energy release at Solfatara volcano, Campi Flegrei, Italy. J. Geophys. Res., 106(B8), 16,213–16,221.

Chiodini, G., Brombach, T., Caliro, S., Cardellini, C., Marini, L., Dietrich, V., 2002. Geochemical indicators of possible ongoing volcanic unrest at Nisyros Island (Greece). Geophys. Res. Lett. 29(16), 1759.

Chiodini, G., Avino, R., Brombach, T., Caliro, S., Cardellini, C., De Vita, S., Frondini, F., Granieri, D., Marotta, E., Ventura, G., 2004. Fumarolic and diffuse soil degassing west of Mount Epomeo, Ischia, Italy. J. Volcanol. Geotherm. Res. 133, 291–309.

Chiodini, G., Granieri, D., Avino, R., Caliro, S., Costa, A., Werner, C., 2005. Carbon dioxide diffuse degassing and estimation of heat release from volcanic and hydrothermal systems. J. Geophys. Res. 110, B08204. doi:10.1029/2004JB003542

Chiodini, G., Baldini, A., Barberi, F., Carapezza, M. L., Cardellini, C., Frondini, F., Granieri, D., Ranaldi, M., 2007. Carbon dioxide degassing at Latera caldera (Italy): Evidence of geothermal reservoir and evaluation of its potential energy. J. Geophys. Res. 112, B12204. doi:10.1029/2006JB004896.

Chiodini, G., Caliro, S., Cardellini, C., Avino, R., Granieri, D., Schmidt, A., 2008. Carbon isotopic composition of soil CO_2 efflux, a powerful method to discriminate different sources feeding soil CO_2 degassing in volcanic-hydrothermal areas. Earth Planet. Sci. Lett. 274, 372–379.

Chiodini, G., Caliro, S., Cardellini, C., Granieri, D., Avino, R., Baldini, A., Donnini, M., Minopoli, C., 2010. Long - term variations of the Campi Flegrei, Italy, volcanic system as revealed by the monitoring of hydrothermal activity. J. Geophys. Res. 115, B03205. doi:10.1029/2008JB006258.

Deutsch, C. V., Journel, A. G., 1998. GSLIB: Geostatistical Software Library and Users Guide. Oxford Univerity Press, New York, 369 pp.

Di Paola, G. M., 1974. Volcanology and Petrology of Nisyros Island (Dodecanese, Greece). Bull. Volcanol. 38, 944-987.

Federman, A. N., Carey, S. N, 1980. Electron microprobe correlation of tephras from eastern Mediterranean abyssal sediments and the island of Santorini. Quaternary Res. 13, 160-171.

Francalanci, L., Varekamp, J. C., Vougioukalakis, G., Defant, M. J., Innocenti, F., Manetti, P., 1995. Crystal retention, fractionation and crustal assimilation in a convecting magma chamber, Nisyros Volcano, Greece. Bull. Volcanol. 56, 601-620.

Fridriksson, T., Kristjánsson, B.R., Ármannsson, H., Margrétardóttir, E., Ólafsdóttir, S., Chiodini, G., 2006. CO_2 emissions and heat flow through soil, fumaroles, and steam heated mud pools at the Reykjanes geothermal area, SW Iceland. Appl. Geochem. 21, 1551–1569.

Frondini, F., Chiodini, G., Caliro, S., Cardellini, C., Granieri, D., Ventura, G., 2004. Diffuse CO_2 degassing at Vesuvio, Italy. Bull. Volcanol. 66, 642-651.

GEOWARN, 2003. GEOWARN geo-spatial warning system—synthesis report GEOWARN consortium Athens (Greece) and Zurich (Switzerland), 57 pp (http://www.geowarn.org).

Giammanco, S., Gurrieri, S., Valenza, M., 1998. Anomalous soil CO_2 degassing in relation to faults and eruptive fissures on Mount Etna (Sicily, Italy). Bull. Volcanol. 60, 252–259.

Gerlach, T. M., Delgado, H., McGee, K. A., Doukas, M. P., Venegas, J. J., Cárdenas, L., 1997. Application of the LI-COR CO_2 analyzer to volcanic plumes: A case study, volcan Popocatepetl, Mexico, June 7 and 10, 1995. J. Geophys. Res. 102, 8005-8019.

Harvey, M. C., Rowland, J. V., Chiodini, G., Rissmann, C. F., Bloomberg, S., Fridriksson, T., Oladottir, A. A., 2017. CO_2 flux geothermometer for geothermal exploration. Geochim. Cosmochim. Acta 213, 1-16. doi: 10.1016/j.gca.2017.06.025

Harvey, M. C., Rowland, J. V., Chiodini G., Rissmann, C. F., Bloomberg, S., Hernandez, P. A., Mazot, A., Viveiros, F., Werner, C., 2015. Heat flux from magmatic hydrothermal systems related to availability of fluid recharge. J. Volcanol. Geotherm. Res. 302, 225–236.

Heidarzadeh M., Necmioglu, O. , Ishibe, T., Yalciner, A. C., 2017. Bodrum–Kos (Turkey–Greece) Mw 6.6 earthquake and tsunami of 20 July 2017: a test for the Mediterranean tsunami warning system. Geosci. Lett. 4:31, doi: 10.1186/s40562-017-0097-0

Hernández, P. A., Pérez, N. M., Salazar, J. M., Nakai, S., Notsu, K., Wakita, H., 1998. Diffuse emission of carbon dioxide, methane, and helium-3 from Teide volcano, Tenerife, Canary Islands. Geophys. Res. Lett. 25, 3311-3314.

Longchamp, C., Bonadonna, C., Bachmann, O., Skopelitis, A., 2011. Characterization of tephra deposits with limited exposure: the example of the two largest explosive eruptions at Nisyros volcano (Greece). Bull. Volcanol. 73, 1337-1352.

Keenan, J. H., Keyes, F. G., Hill, P. G., Moore, J. G., 1969. Steam- Tables: Thermodynamic Properties of Water Including Vapor, Liquid and Solid Phases. International Edition Metric Units, John Wiley, New York 162 pp.

Kerrick, D. M., McKibben, M. A., Seward, T. M., Caldeira, K., 1995, Convective hydrothermal CO_2 emission from high heat-flow regions, Chem. Geol., 121, 285– 293.

Marini, L., Fiebig, J., 2005. Fluid geochemistry of the magmatic-hydrothermal system of Nisyros (Aegean arc, Greece). In: Hunziker, J.C., Marini, L. (Eds.), The Geology, Geochemistry and Evolution of Nisyros Volcano (Greece); Implications for the Volcanic Hazards: Memoires de Geologie (Lausanne), 44, pp. 121–163.

Marini, L., Principe, C., Chiodini, G., Cioni, R., Fytikas, M., Marinelli, G., 1993. Hydrothermal eruptions of Nisyros (Dodecanese, Greece). Past events and present hazard. J. Volcanol. Geotherm. Res. 56, 71–94.

Matsuda, J., Senoh, K., Maruoka, T., Sato, H., Mitropoulos, P., 1999. K-Ar ages of the Aegean volcanic rocks and their implication for the arc-trench system. Geochem. J. 33, 369-377.

Mori, T., Hernández, P. A., Salazar, J. M. L., Pérez, N. M., Notsu, K., 2001. An in situ method for measuring CO_2 flux from volcanic-hydrothermal fumaroles. Chem. Geol. 177, 85-99.

Papadimitriou, P., Karakonstantis, A., Kapetanidis, V., Bozionelos, G., Kaviris, G., Voulgaris, N., 2017. Seismicity and Tomographic Imaging of the Broader Nisyros Region (Greece). In: Dietrich, V. J., Lagios, E. (Eds.), Nisyros Volcano, the Kos - Yali - Nisyros Volcanic Field: Springer, pp. 245-272.

Papadopoulos, G. A., Sachpazi, M., Panopoulou, G., Stavrakakis, G., 1998. The volcanoseismic crisis of 1996–97 in Nisyros, SE Aegean Sea, Greece. Terra Nova 10(3), 151–154.

Pe-Piper, G., Piper, D. J. W., 2002. The igneous rocks of Greece. Berlin: Gebrüder Borntreager.

Pérez, N. M., Hernández, P. A., Padilla, G., Nolasco, D., Barrancos, J., Melían, G., Padrón, E., Dionis, S., Calvo, D., Rodríguez, F., Notsu, K., Mori, T., Kusakabe, M., Arpa, M.C., Reniva, P., Ibarra, M., 2011. Global CO_2 emission from volcanic lakes. Geology 39, 235-238.

Pérez, N. M., Hernández, P. A., Padrón, E., Melían, G., Nolasco, D., Barrancos, J., Padilla, G., Calvo, D., Rodríguez, F., Dionis, S., Chiodini, G., 2013. An increasing trend of diffuse CO_2 emission from Teide volcano (Tenerife, Canary Islands): geochemical evidence of magma degassing episodes. J. Geol. Soc., London 170(4), 585-592. doi:10.1144/jgs2012-125.

Poland, M. P., Miklius, A., Sutton, A. J., Thornber, C. R., 2012. A mantle-driven surge in magma supply to Kilauea Volcano during 2003-2007. Nat. Geosci. 5, 295-U297.

Sachpazi, M., Kontoes, C., Voulgaris, N., Laigle, M., Vougioukalakis, G., Olga Sikioti, G., Stavrakakis, G., Baskoutas, J., Kalogeras, J., Lepine, J., 2002. Seismological and SAR signature of unrest at Nisyros caldera, Greece. J. Volcanol. Geoth. Res. 116, 19–33.

Schütze, C., Vienken, T., Werban, U., Dietrich, P., Finizola, A., Leven, C., 2012. Joint application of geophysical methods and Direct Push-soil gas surveys for the improved delineation of buried fault zones. J. Appl. Geophys. 82, 129-136, doi: 755 10.1016/j.jappgeo.2012.03.002.

Sinclair, A. J., 1974. Selection of threshold values in geochemical data using probability graphs. J. Geochem. Explor. 3, 129–149.

Smith, P. E., York, D., Chen, Y., Evensen, N. M., 1996. Single crystal $^{40}Ar/^{39}Ar$ dating of a late Quaternary paroxysm on Kos, Greece; concordance of terrestrial and marine ages. Geophys. Res. Lett. 23, 3047-3050.

Sorey, M.L., 1985, Evolution and present state of the hydrothermal system in Long Valley caldera: J. Geophys. Res., 90(B13), 11,219–11,228.

Venturi, S., Tassi, F., Vaselli, O., Vougioukalakis, G. E., Rashed, H., Kanellopoulos, C., Caponi, C., Capecchiacci, F., Cabassi, J., Ricci, A., Giannini, L., 2018. Active hydrothermal fluids circulation triggering small- scale collapse events: the case of the 2001–2002 fissure in the Lakki Plain (Nisyros Island, Aegean Sea, Greece). Nat. Hazards. doi: 10.1007/s11069-018-3318-8.

Viveiros, F., Ferreira, T., Cabral Vieira, J., Silva, C., Gaspar, J. L., 2008. Environmental Influences on soil CO_2 degassing at Furnas and Fogo volcanoes (Sao Miguel Island, Azores archipelago). J. Volcanol. Geotherm. Res. 177, 883–893. doi: 10.1016/j.jvolgeores.2008.07.005.

Viveiros, F., Cardellini, C., Ferreira, T., Caliro, S., Chiodini, G., Silva, C., 2010. Soil CO_2 emissions at Furnas volcano, Sao Miguel Island, Azores archipelago: volcano monitoring perspectives, geomorphologic studies, and land use planning application. J. Geophys. Res. 115, B12208. doi:10.1029/2010JB007555.

Vougioukalakis, G., 1993. Volcanic stratigraphy and evolution of Nisyros island. Bull. Geol. Soc. Greece XXVIII, 239–258.

Vougioukalakis, G., 1998. Blue volcanoes: Nisyros. Regional Council of Mandraki.

Vougioukalakis, G., Androulakakis, N., 2008. Presenting the Volcano of Nisyros. http://nisyros.igme.gr/nisyros/index.php?option=com_content&task=view&id=12&Itemid=26, Athens, IGME.

Wagner, G. J., Storzer, D., Keller, J., 1976. Spaltspurendatierungen quartarer Gesteinsglaser aus dem Mittelmeerraum ¨. Neues Jahrb. Miner. Monatsh. 2, 84-94.

Werner, C. and Cardellini, C., 2006. Comparison of carbon dioxide emissions with fluid upflow, chemistry, and geologic structures at the Rotorua geothermal system, New Zealand. Geothermics 35, 221–238.

Werner, C., Bergfeld, D., Farrar, C. D., Doukas, M. P., Kelly, P. J., Kern, C., 2014. Decadal-scale variability of diffuse CO_2 emissions and seismicity revealed from long-term monitoring (1995-2013) at Mammoth Mountain, California, USA. J. Volcanol. Geotherm. Res. 289, 51-63.

Werner, C., Fischer, T. P., Aiuppa, A., Edmonds, M., Cardellini, C., Carn, S., Chiodini, G., Cottrell, E., Burton, M., Shinohara, H., Allard, P., 2019. Carbon dioxide emissions from subaerial volcanic regions: Two decades in review, in Daniel, I., Rajdeep, D., and Orcutt, B. eds., Whole Earth Carbon: Past to Present, Cambridge University Press, in press.

Fig. 1. a) The volcanoes of the Aegean arc and location of Nisyros. b) Simplified geological map of Nisyros redrawn from Vougioukalakis and Androulakakis (2008).

Fig. 2. Conceptual model of a convective hydrothermal system used for the computation of the H_2O mass and energy balances. Q_i and QH_i are the mass and thermal energy fluxes of the deep original liquid (subscript *L0*), of the residual liquid remaining after boiling (subscript *res*) and of the steam separated during the boiling that condense in the subsurface (subscript *cond*).

Fig. 3. Map of soil CO_2 flux at Lakki plain realised based on the October 2018 survey. The map was realised by averaging the results of 200 sequential Gaussian simulation over a grid of 317×408 cells of 5×5 m. The white rectangular indicates the zone where the background was computed (see text for further explanations). The coordinates refer to the WGS 84/UTM zone 35 S.

Fig. 4. (a) Log probability plot of soil CO_2 fluxes measured in the NE sector of the study area (see Fig.2 and the text for further explanations) and (b) probability plot of $\delta^{13}C$ soil CO_2 composition (data from Venturi et al., 2018)

Fig. 5. Probability maps realised using 200 sequential Gaussian simulations. The colours refer to the probability that, among all the realizations, the simulated CO_2 flux at any location is above the cut-off value of 15 g m^{-2} d^{-1}. The map highlights the areas where the CO_2 flux is fed by the hydrothermal source because the selected cut-off is a maximum value for the background (biogenic) CO_2 flux (see Fig. 3 and the text). The maps show the main volcanic-hydrothermal and tectonic features of Lakki plain (redraw from Caliro et al., 2005) and the most evident lineaments (dashed lines) highlighted by CO_2 fluxes. In the map are reported also the nine DDSs that are treated one by one (see table 2).

Fig. 6. Extent (a) and total CO_2 output (b) of the nine DDSs in 2018 compared with the same data of the 1999-2001 surveys.

Fig. 7. Maps of soil CO_2 flux in the area of the 2001-2002 fracture. Panel a) refers to the general data set while the map in panel b) was realised considering also 30 points specifically measured at the bottom of the fracture. Panel c shows the soil CO_2 flux transects c1-c10 whose location is reported in panel b.

Fig. 8. The CO_2 molalities and temperatures estimated for Nis-1 and Nis-2 wells (Marini and Fiebig, 2005) are compared with the T- m_{CO2} empirical relation valid for many geothermal systems of the world (Arnorsson and Gunnlaugsson, 1985). The horizontal lines refer to the convective flux of original liquids computed for different CO_2 concentrations and for the 2018 total hydrothermal CO_2 emission of 91.6 t/d. See the text for further explanations.

Table 1. Results of the 2018 survey (DDS extent and Total CO_2 output) compared with the results obtained for the 1999-2001 survey.

Date	Investigated area (km^2)	Total CO_2 output (t/d)	Hydrothermal CO_2 output (t/d)	DDSs Extent km^2
1999-2001	1.97	81.6±6.8	73.7	0.77
2018	2.22	100.6±7.9	91.6	0.92

Table 2. Number of measurements (n.), hydrothermal CO_2 output and extent of the nine DDSs of Nisyros (see Fig. 4 and Appendix d). The 2018 results are compared with those of the 1999-2001 surveys.

	1999-2001			2018		
Name	n.	CO_2 output (t/d)	Extent (km^2)	n.	CO_2 output (t/d)	Extent (km^2)
1-Stefanos	232	14.7±1.9	0.063	162	16.8±1.6	0.086
2-Kaminakia	241	20.8±1.0	0.130	112	13.4±1.5	0.164
3-Polybote	117	6.61±0.73	0.035	49	5.59±1.42	0.031
4-Phlegeton	178	4.87±0.68	0.047	79	3.44±0.41	0.053
5-Lofos	517	12.6±0.8	0.154	146	20.0±2.1	0.196
6-Ramos	102	4.83±0.66	0.057	74	10.5±2.2	0.048
7-NEfault	305	3.99±0.0.28	0.092	124	8.27±1.2	0.098
8-NESWline	281	2.90±0.11	0.097	194	4.11±0.15	0.120
9-NWSEline	188	0.86±0.08	0.015	134	1.86±0.17	0.029

Table 3. Thermal emission by condensation of the steam (QH_{cond}) computed for the nine DDSs of Nisyros. The ratio H_2O/CO_2 ($R_{H2O/CO2}$) refers to the fumaroles located in the DDS or to the closest fumaroles (Chiodini et al., 1993; Brombach et al., 2003; Caliro et al., 2005). The Total (DDSs) is the sum of the contributions from the nine DDSs, while the Total Area values were scaled to the entire surveyed area

Name	Q_{CO2} (kg/s)	$R_{H2O/CO2}$ $\pm 1\sigma$	Q_{cond} (kg/s)	QH_{cond} (MW)
1-Stefanos	0.194	36.0 ± 4.2	7.00	18.1
2-Kaminakia	0.155	6.9 ± 2.6	1.08	2.8
3-Polybote	0.065	26.0 ± 5.1	1.68	4.4
4-Phlegeton	0.040	21.2 ± 4.0	0.85	2.2
5-Lofos	0.231	27.3 ± 2.3	6.31	16.4
6-Ramos	0.122	16.5 ± 2.6	2.01	5.2
7-NEfault	0.096	6.9 ± 2.6	0.66	1.7
8-NESWline	0.048	27.3 ± 2.3	1.30	3.4
9-NWSEline	0.022	27.3 ± 2.3	0.59	1.5
Total (DDSs)	0.972		21.5	55.7
Total Area	1.060		23.4	60.7

Table 4. Water mass and thermal budget of the process generating the soil emission of hydrothermal CO_2 at Lakki plain assuming the original temperature and CO_2 molality equal to that of Nis-1 and Nis-2 geothermal wells.

Well name	Q_{CO2} (kg/s)	Q_{L0} (kg/s)	Q_{cond} (kg/s)	Q_{res} (kg/s)	QH_{L0} (MW)	QH_{cond} (MW)	QH_{res} (MW)
Nis-1	1.06	83.9	23.4	61.0	134	60.7	74.4
Nis-2	1.06	208.5	23.4	185.6	270	60.7	211

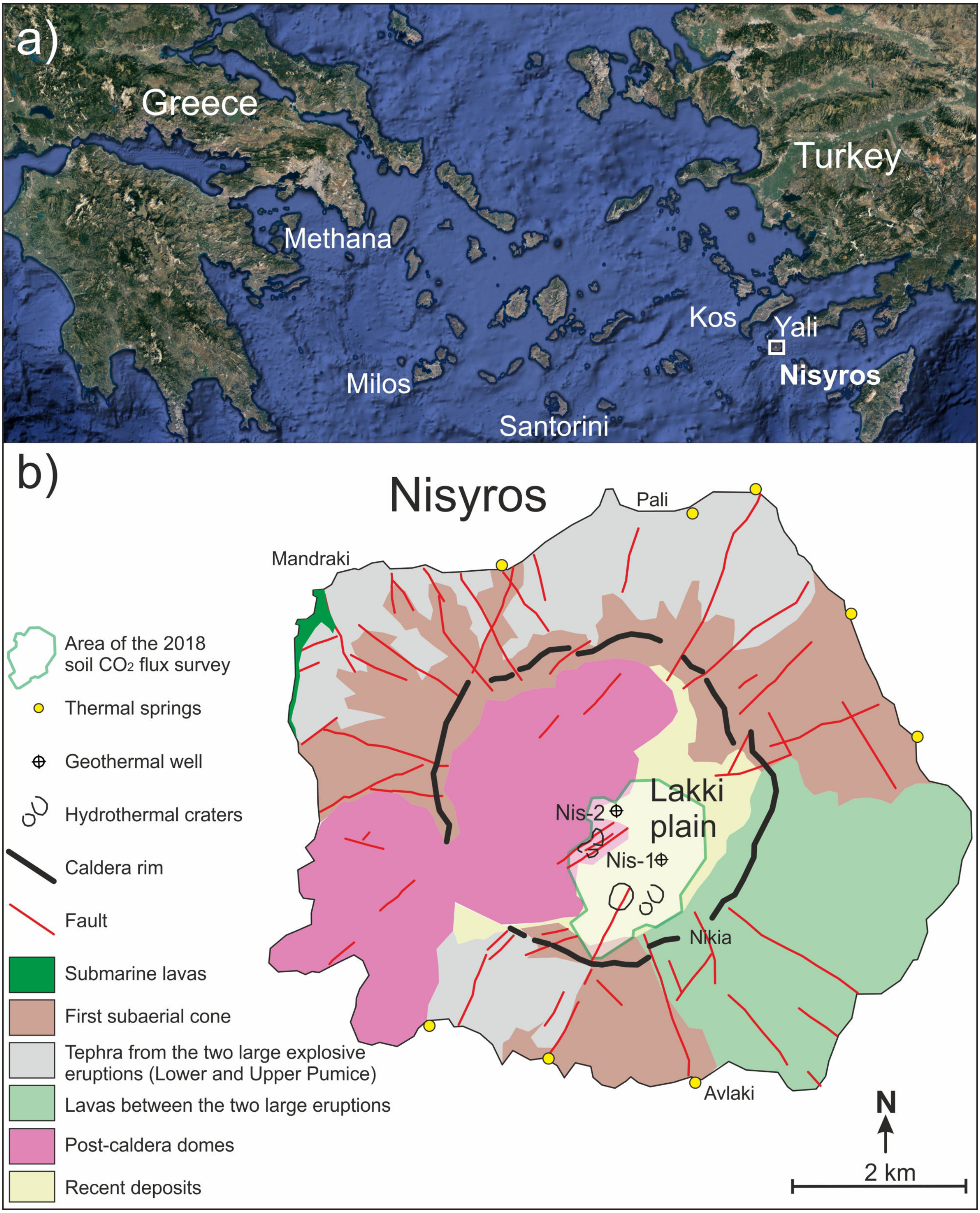
a)
Greece
Turkey
Methana
Kos
Yali
Nisyros
Milos
Santorini
b)
Nisyros
Pali
Mandraki
Lakki plain
Nis-2
Nis-1
Nikia
Avlaki
Area of the 2018 soil CO$_2$ flux survey
Thermal springs
Geothermal well
Hydrothermal craters
Caldera rim
Fault
Submarine lavas
First subaerial cone
Tephra from the two large explosive eruptions (Lower and Upper Pumice)
Lavas between the two large eruptions
Post-caldera domes
Recent deposits
N
2 km

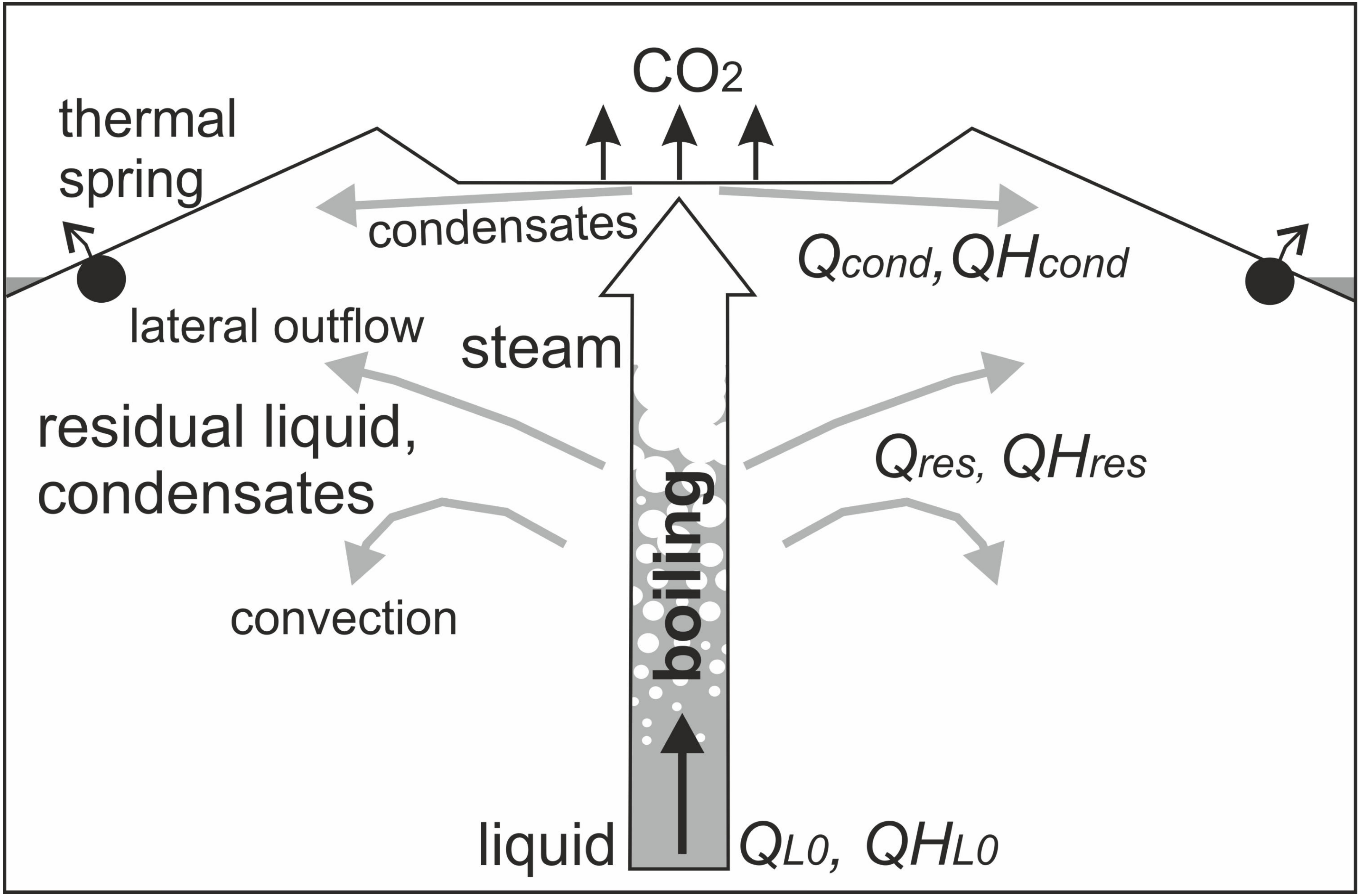
CO2
thermal spring
condensates
Qcond, QHcond
lateral outflow
steam
residual liquid, condensates
Qres, QHres
boiling
convection
liquid
QL0, QHL0

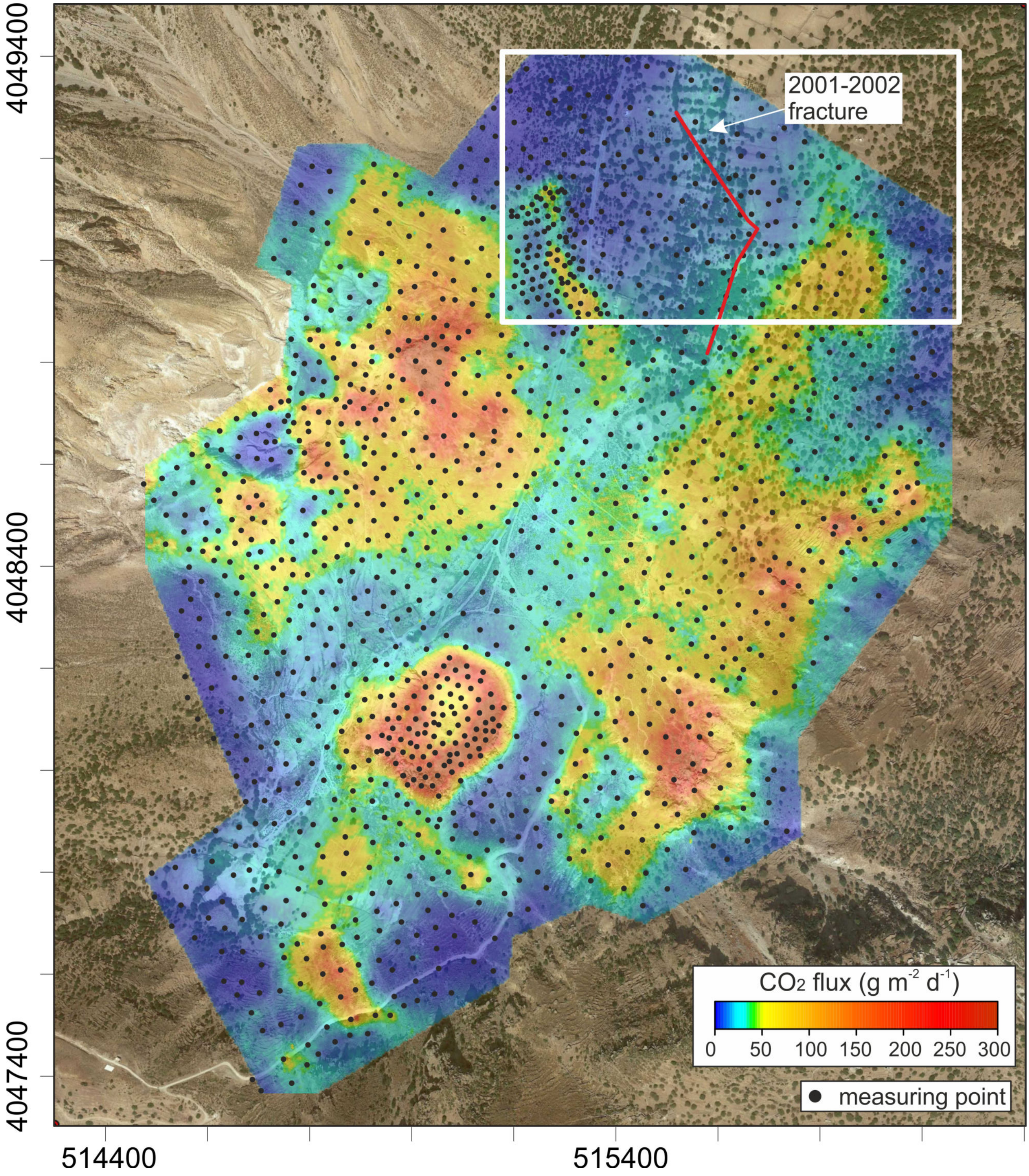
4049400
4048400
4047400
514400
515400
2001-2002 fracture
CO2 flux (g m-2 d-1)
0
50
100
150
200
250
300
measuring point

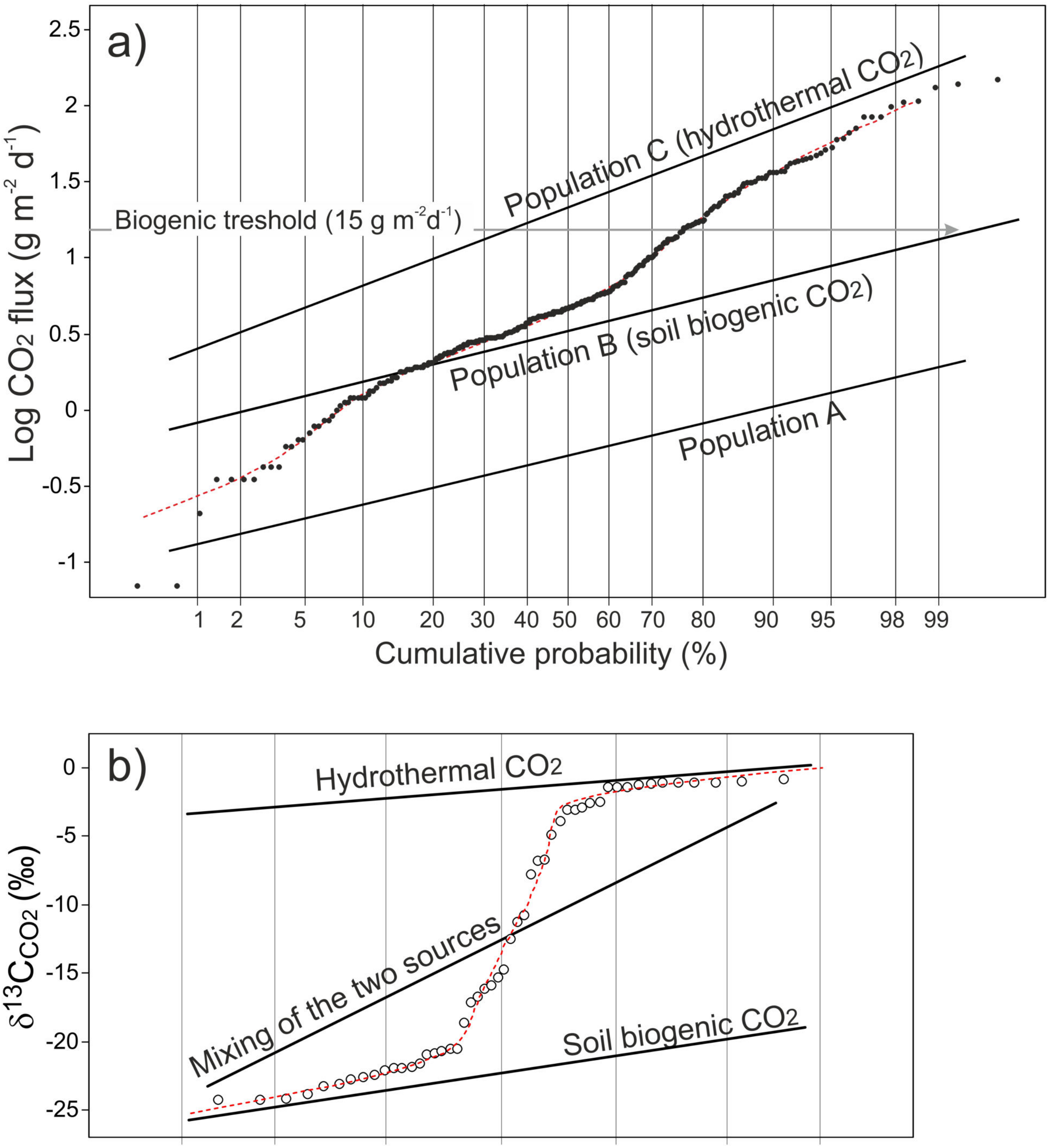
a)
Log CO2 flux (g m-2 d-1)
2.5
2
1.5
1
0.5
0
-0.5
-1
Population C (hydrothermal CO2)
Biogenic treshold (15 g m-2d-1)
Population B (soil biogenic CO2)
Population A
1
2
5
10
20
30
40
50
60
70
80
90
95
98
99
Cumulative probability (%)
b)
δ13C CO2 (‰)
0
-5
-10
-15
-20
-25
Hydrothermal CO2
Mixing of the two sources
Soil biogenic CO2
1
5
20
50
80
95
99
Cumulative probability (%)

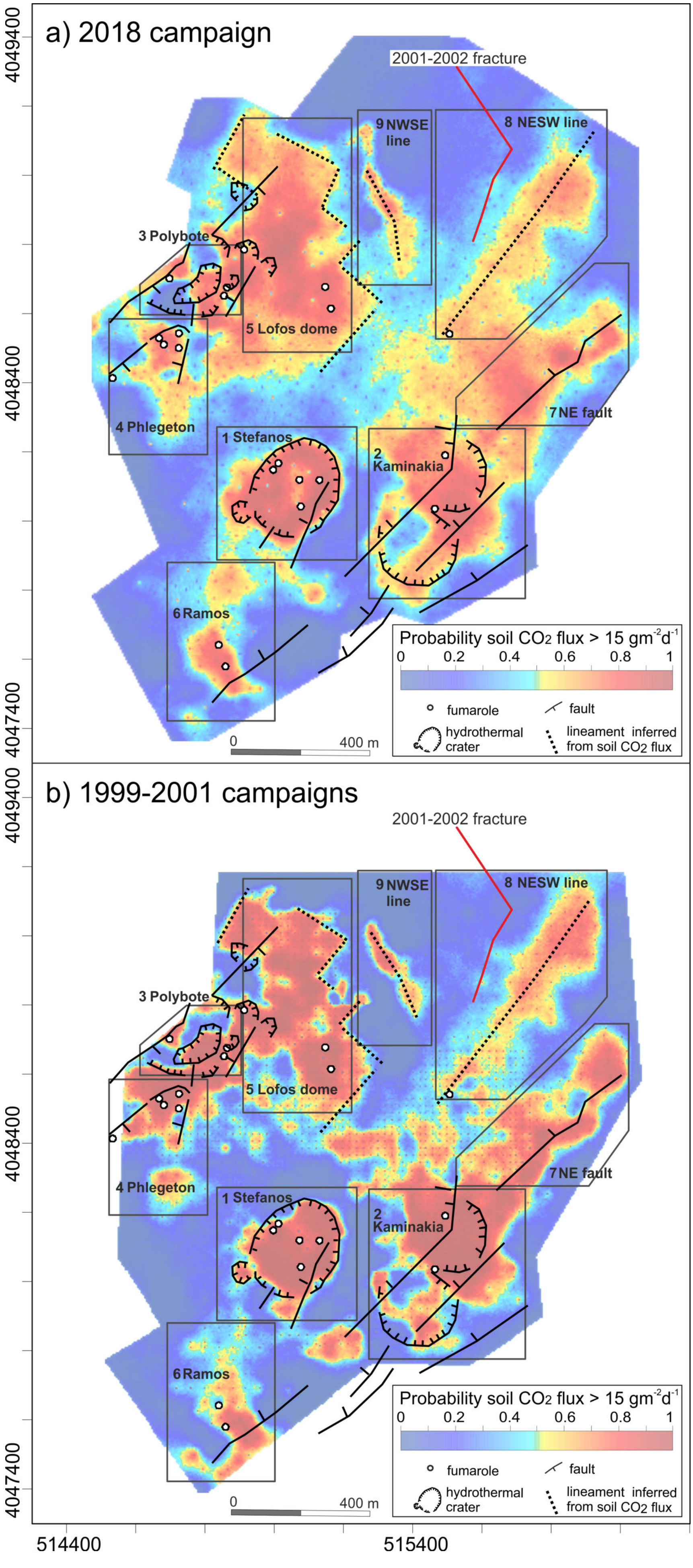
a) 2018 campaign
b) 1999-2001 campaigns
2001-2002 fracture
1 Stefanos
2 Kaminakia
3 Polybote
4 Phlegeton
5 Lofos dome
6 Ramos
7 NE fault
8 NESW line
9 NWSE line
Probability soil CO2 flux > 15 gm-2d-1
0
0.2
0.4
0.6
0.8
1
fumarole
fault
hydrothermal crater
lineament inferred from soil CO2 flux
0
400 m
4049400
4048400
4047400
514400
515400

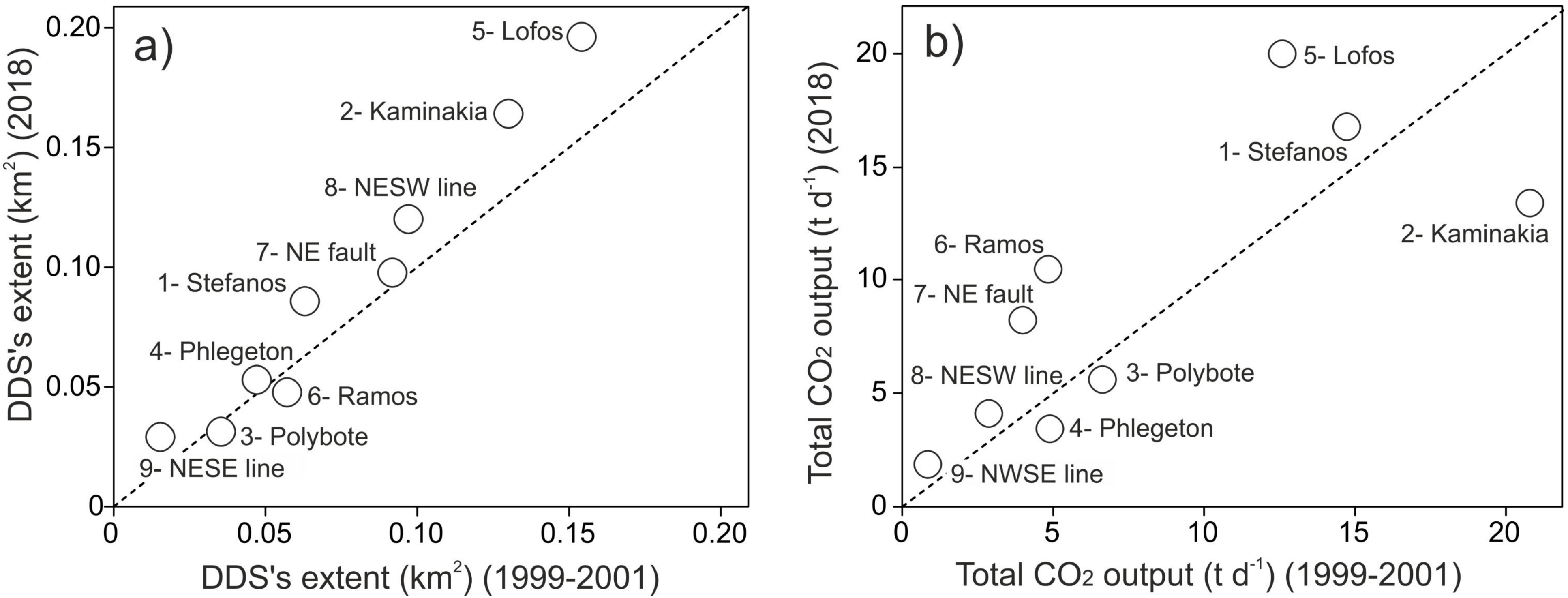
a)
5- Lofos
2- Kaminakia
8- NESW line
7- NE fault
1- Stefanos
4- Phlegeton
6- Ramos
3- Polybote
9- NESE line
0.20
0.15
0.10
0.05
0
0
0.05
0.10
0.15
0.20
DDS's extent (km^2) (2018)
DDS's extent (km^2) (1999-2001)
b)
5- Lofos
1- Stefanos
2- Kaminakia
6- Ramos
7- NE fault
8- NESW line
3- Polybote
4- Phlegeton
9- NWSE line
20
15
10
5
0
0
5
10
15
20
Total CO$_2$ output (t d^{-1}) (2018)
Total CO$_2$ output (t d^{-1}) (1999-2001)

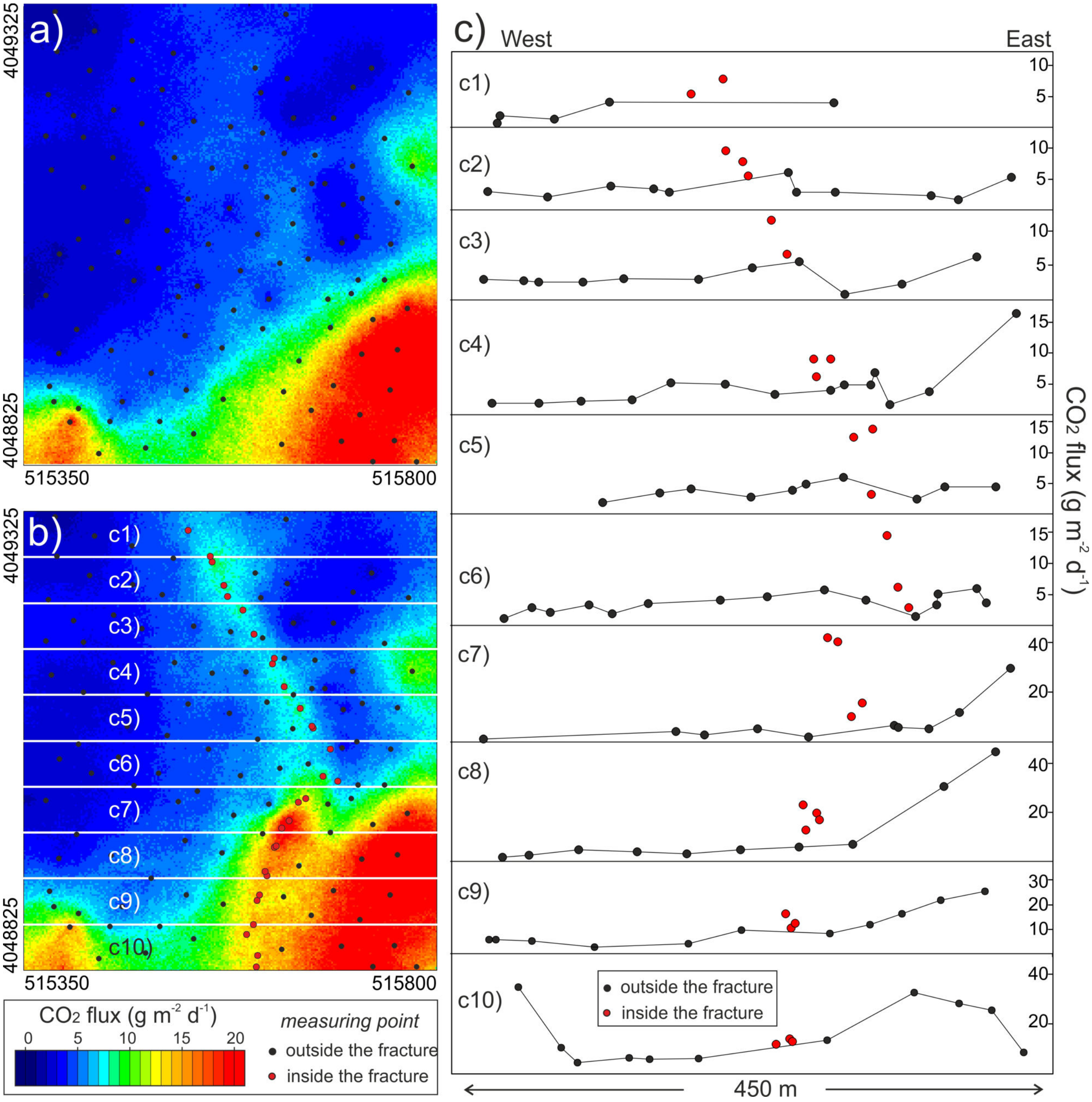
a)
4049325
4048825
515350
515800
b)
c1)
c2)
c3)
c4)
c5)
c6)
c7)
c8)
c9)
c10)
4049325
4048825
515350
515800
CO2 flux (g m-2 d-1)
0
5
10
15
20
measuring point
outside the fracture
inside the fracture
c)
West
East
c1)
10
5
c2)
10
5
c3)
10
5
c4)
15
10
5
c5)
15
10
5
c6)
15
10
5
c7)
40
20
c8)
40
20
c9)
30
20
10
c10)
40
20
outside the fracture
inside the fracture
CO2 flux (g m-2 d-1)
450 m

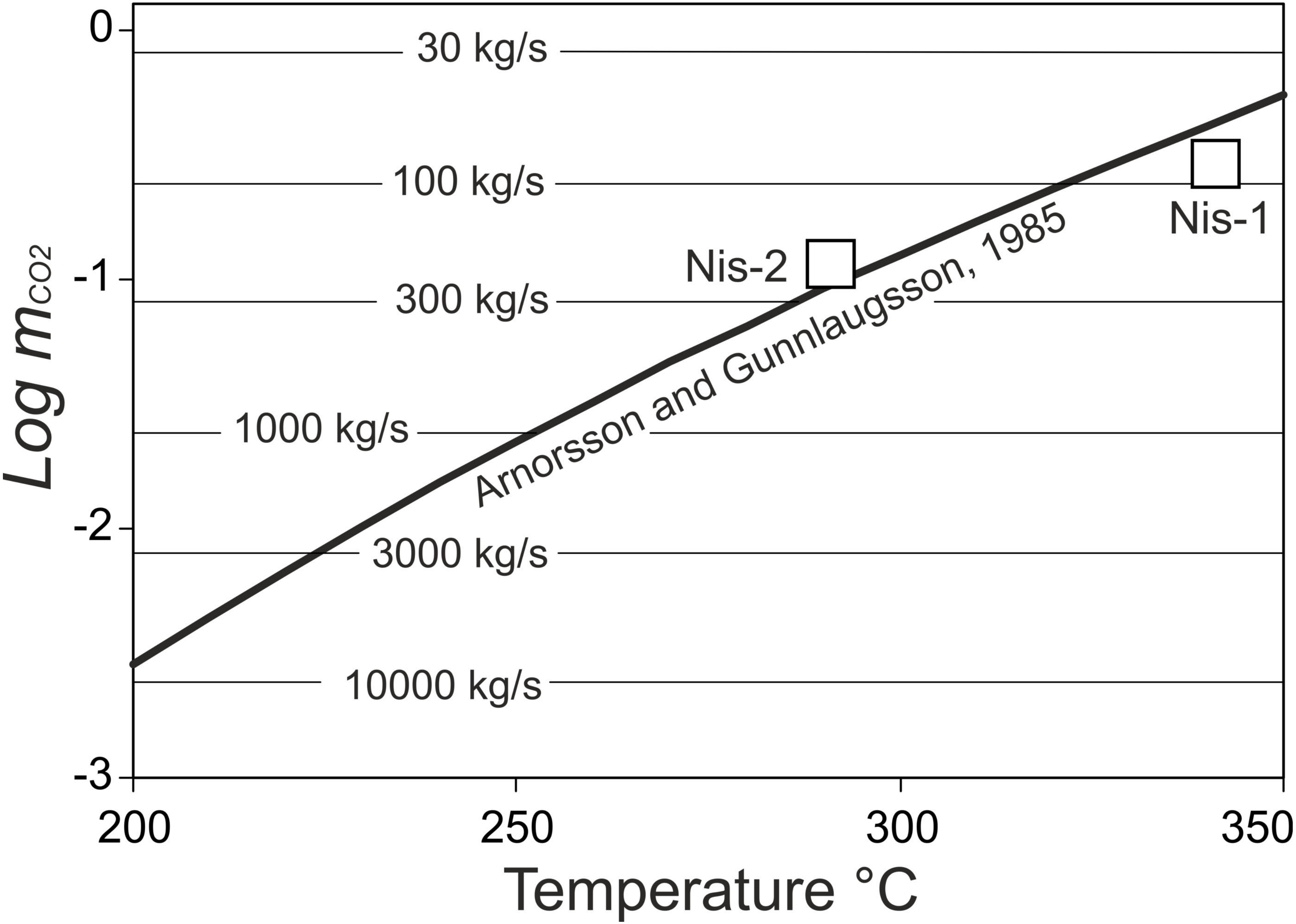

30 kg/s
100 kg/s
300 kg/s
1000 kg/s
3000 kg/s
10000 kg/s
Nis-1
Nis-2
Arnorsson and Gunnlaugsson, 1985
0
-1
-2
-3
Log m_{CO2}
200
250
300
350
Temperature °C